Design and Validation of Flim-timer for Measuring Protein Turnover in Cells Using Fluorescence Lifetime

Dina Dikovskaya (ddikovskaya@dundee.ac.uk)
University of Dundee https://orcid.org/0000-0003-3161-3072
Claudia Bento-Pereira
University of Dundee
Kanade Shiga
University of Dundee
Andrea Corno
University of Dundee https://orcid.org/0000-0002-7748-7561
Maureen Higgins
University of Dundee
Rachel Toth
University of Dundee https://orcid.org/0000-0002-1337-0612
Adrian Saurin
University of Dundee https://orcid.org/0000-0001-9317-2255
Albena Dinkova-Kostova
University of Dundee https://orcid.org/0000-0003-0316-9859

Article

Keywords:

Posted Date: January 17th, 2024

DOI: https://doi.org/10.21203/rs.3.rs-2161438/v1

Additional Declarations: There is **NO** Competing Interest.

DESIGN AND VALIDATION OF FLIM-TIMER FOR MEASURING PROTEIN TURNOVER IN CELLS USING FLUORESCENCE LIFETIME.

Dina Dikovskaya[1,2,*], Claudia Bento-Pereira[1], Kanade Shiga[1,3], Andrea Corno[1], Maureen Higgins[1], Rachel Toth[4], Adrian T. Saurin[1] and Albena T. Dinkova-Kostova[1,5].

[1]Division of Cellular Medicine, University of Dundee School of Medicine, Dundee, DD1 9SY, United Kingdom
[2]MRC Protein Phosphorylation and Ubiquitylation Unit, University of Dundee, Dundee DD1 5EH, United Kingdom
[3]The Department of Advanced Health Science, Graduate School of Advanced Health Sciences, Saga University
[4]MRC Reagents and Services, University of Dundee, Dundee, DD1 5EH, United Kingdom
[5]Department of Pharmacology and Molecular Sciences and Department of Medicine, Johns Hopkins University School of Medicine, Baltimore, MD, USA
[*]corresponding author

Abstract

Measuring protein turnover in individual cells and subcellular compartments has been greatly assisted by fluorescence timers (FT) whose changing spectra, expressed as the ratio of fluorescence intensities, reflect their molecular age. However, FT quantification requires highly fluorescent samples, prohibiting their use for proteins with low or non-uniform expression. Here we developed a method that utilises fluorescence lifetime, a property largely independent of intensity, of a specifically designed FT (named FLIM-timer). The fluorescence lifetime of FLIM-timer reflected protein turnover in regions of high and low brightness with equally high precision. We demonstrate the versatility of this approach with several versions of FLIM-timer in two distinct experimental systems: 1) as a readout for efficacy of pharmacological inducers of Nrf2, the master regulator of redox homeostasis, and 2) as a tool to monitor cyclin B1 degradation during mitotic exit. Overall, the FLIM-timer methodology expands the applicability of FT for visualisation and quantification of protein turnover.

Introduction

Protein turnover, the balance between protein synthesis and degradation, is fundamental for normal cellular function and is frequently altered in disease. The appropriate time and location of protein degradation is extremely important for healthy functioning of cells and organisms, and its understanding requires methods that assess protein half-life at subcellular resolution. Fluorescence Timers (FT), fluorescent molecules that change their spectra over time, allow assessment of protein turnover and trafficking within live cells or an organism at cellular and subcellular resolution[1-4]. Since the colour of FT reflects the time elapsed from its synthesis, the stability or retention of FT-tagged protein within a cellular compartment can be inferred from the amount of fluorescence measured at the wavelength that corresponds to the converted (late) FT, relative to the fluorescence intensity in the initial FT spectra. Thus, the ratio between converted and initial fluorescence intensities serves as FT readout, with low values indicating high turnover, and *vice versa*.

While the FT approach has a high spatial resolution typical for microscopy-based applications, its quantitative aspect is limited due to the ratiometric nature of the measurements that lose precision at low initial FT intensity used as a denominator. This is particularly problematic for targets with low or non-uniform expression levels. To overcome this limitation, we now report the development of an alternative protein turnover measurement technique based on fluorescence lifetime, the time between excitation and emission, that is independent of the expression level of the fluorescent protein [5].

Results

Generation of FLIM-timer as a readout for protein turnover

To expand the use of FT to systems with weak/variable levels of target proteins, we constructed a genetically encoded protein tag in which we combined two fluorophores capable of Förster Resonance Energy Transfer (FRET) between them, connected by a short linker that positions the fluorophores in a way that promotes FRET [6, 7](**Fig. 1a**), and employed Fluorescence Lifetime Imaging (FLIM) to measure FRET between the tag components. FRET reduces fluorescence lifetime, the time between excitation and emission, of the fluorophore acting as a FRET donor, and this reduction is independent of the amount of the FRET donor and proportional to the FRET efficiency [8, 9]. Consequently, fluorescence lifetime measurements using FLIM provide a highly sensitive and quantitative readout for FRET.

To achieve time-dependent changes in FLIM-FRET, we took advantage of the previously developed concept of tandem fluorescence timer (tFT) [4] that combines fluorophores with different maturation times, i.e. the times during which the newly synthesized fluorophores are spontaneously rearranged to become fluorescent [10, 11]. In this system, the difference between the onset of fluorescence for the two tag components creates a time window in which the intensity of the fast-maturing fluorophore is constant, while the intensity of the slow-maturing fluorophore increases over time, changing the ratio between their fluorescence intensity with time, similar to that observed in single-molecule FT.

We hypothesised that the ability of a fluorophore to accept FRET is dependent on its maturation state. If our hypothesis is correct, the combination of a FRET donor with fast maturation and a FRET acceptor with slow maturation should lead to a minimal intra-tag FRET in the newly synthesized protein that increases over time as a result of FRET acceptor maturation. Consequently, the fluorescence lifetime of the FRET donor within such tag (referred further as FLIM-timer) could serve as readout for protein turnover, with its highest values corresponding to high turnover/unstable protein, and *vice versa*.

To test this idea, we selected sfGFP [12] or mNeonGreen [13] , both of which have fast intrinsic maturation, as FRET donors, and mCherry , which has a slower maturation kinetics, as a FRET acceptor [11], a fluorophore combination previously used for tFT in yeast [4, 14]. We confirmed the efficient FRET between sfGFP and mCherry and between mNeonGreen and mCherry, as seen by a strongly reduced fluorescence lifetimes of sfGFP and mNeonGreen in the context of the tag, compared to that without mCherry (**Fig. 1b**), with average FRET efficiency 12.13% for sfGFP-based FLIM-timer and 12.78% for mNeonGreen-based FLIM-timer. The differences between the maximal and minimal fluorescence lifetimes were approximately 350 ps for sfGFP-based FRET pair and 380 ps for mNeonGreen-based FRET

pair, providing sufficient resolution for monitoring changes in protein stability using FLIM. Note that intrinsic turnover rates of both composite tags are much slower than the known maturation rate of mCherry [11], therefore these tags on their own could be considered as stable proteins.

To determine whether fluorescence lifetime of such tag is sensitive to changes in protein stability, we generated a fusion of sfGFP-based FLIM-timer with Nrf2, a transcription factor that regulates the cellular redox homeostasis. At basal conditions, endogenous Nrf2 is an extremely unstable protein with a half-life of about 20 min, due to a Keap1-dependent degradation [15, 16]. Remarkably, mCherry/sfGFP intensity ratio (previously used measure for turnover of tFT-tagged proteins) in cells transiently transfected with this construct strongly negatively correlated with the fluorescence lifetime (denoted further as tm) of the FRET donor sfGFP (**Fig. 1c**). This is consistent with maturation-dependent changes in FRET efficiency of the FLIM-timer and confirms that fluorescence lifetime of FLIM-timer-tagged proteins can be used as readout of their turnover.

The strong correlation with high goodness of fit was observed regardless whether fluorescence livetime was determined by fitting one-component or two-component exponential decay model (compare **Fig. 1c and Suppl Fig. 1a**), and was also apparent between mCherry/sfGFP intensity ratio and FRET efficiency of FLIM-timer (**Suppl Fig. 1b**). While the more complex model showed a statistically significant improvement of fit, the difference in the goodness of fit between these models was very small (**Suppl Fig 1c**). Therefore, the minimal one-component fit for fluorescence lifetime measurements was deemed adequate and was adopted for the rest of this study.

Improved precision and visibility of fluorescence lifetime-based timer.
To compare FLIM-based and ratiometric measurements, we calculated the mean values and variability for each type of measurement among pixels of different intensities within the same cell. In order to uncouple the pixel brightness (potentially linked to the local protein stability) from the FT readouts, we replaced sfGFP within FT by EGFP (**Fig. 1d**). This construct is not sensitive to fluctuations in protein turnover since the maturation time of EGFP is close to that of mCherry. Consistent with the notion that fluorescence lifetime is largely independent of the level of FRET donor, the average GFP fluorescence lifetime in the cell transfected with EGFP-mCherry plasmid was similar among pixels with low and high intensities (**Suppl Fig.1d**, blue line in the inset). In contrast, the average mCherry/GFP intensity ratio in the same cell was higher for pixels with low GFP intensity (**Suppl Fig.1e)**, blue line in the inset). The variability of fluorescence lifetime among pixels was overall much lower than that of mCherry/GFP intensity ratio, with mean Relative Standard Deviation equal 1.99% for tm (1.45% for pixels with intensities above background) and 46.77% for the ratiometric values (32.56% for pixels with intensities above background) (**Fig. 1e**). Importantly, there was very little, if any, difference in fluorescence lifetime variability among dim and bright pixels of the image, while the mCherry/EGFP intensity ratio predictably showed a dramatic increase in variability at the lower intensity range (**Fig. 1e**). FLIM also improved visualisation of stability/turnover of FLIM-timer-tagged Nrf2 overexpressed in HeLa cells (**Fig. 1f**), as it produced a high-contrast map in regions of both high and low levels of tagged protein. Thus, FLIM-based measurements of fluorescence

timer are superior to the currently available ratiomeric measurement approach in several ways.

Applications of FLIM-timer

1. *Monitoring drug-induced Nrf2 stabilization.*

Initiation of the oxidative stress response is driven by stabilisation of Nrf2 protein as a result of inhibitory modification of the sensor cysteines of its negative regulator Keap1 by oxidants or electrophiles, collectively called Nrf2 inducers [17] (**Fig. 2a**). Nrf2 activation allows for adaptation and survival under stress conditions and has shown protective effects in many preclinical models of human disease and in clinical trials. A growing number of pharmacological Nrf2 inducers are in various stages of drug development to counteract oxidative stress, toxicity and inflammation in a number of chronic diseases [18, 19]. We wanted to see whether FLIM-timer-tagged Nrf2 could be used to detect Nrf2 activation, by reporting on stabilisation of Nrf2 protein. N-terminally FLIM-timer-tagged Nrf2 overexpressed in HeLa cells localised predominantly to the nucleus (**Fig. 2b**), as previously observed for a transiently transfected fluorescently-labelled Nrf2 [7]. Our previous work confirmed that N-terminally tagged Nrf2 remains transcriptionally active and retains Keap1-dependent regulation [7, 20]. In the absence of any treatment, the fluorescence lifetime of nuclear FT-Nrf2 was much shorter than that in the cytoplasm, indicative of low turnover of Nrf2 protein in the nucleus and its high turnover in the cytoplasm (**Fig. 2b** and **Suppl. Fig 2a-b**). The reduced nuclear fluorescence lifetime was unique to FT-Nrf2 and not observed for sfGFP-Nrf2 expressed with or without free mCherry, or for Nrf2 tagged with sfGFP at its N-terminus and with mCherry at its C-terminus, the tagging strategy that can act as ratiometric fluorescence timer but not as FLIM-timer (**Fig. 2b**). Surprisingly, treatment of cells with an established Nrf2 inducer sulforaphane (SFN) [18] that targets Keap1 did not stabilise the overexpressed FT-Nrf2 (**Suppl. Fig 2c**), though the level of endogenous Nrf2 was increased by the same treatment (**Suppl. Fig 2c,** bottom left panel). One possible explanation for this result is that visible amounts of overexpressed FT-Nrf2 much exceed that of endogenous Nrf2, and that endogenous level of Keap1 is insufficient to regulate such excess of Nrf2. Consequently, the modification of endogenous Keap1 with sulforaphane would have little effect on the stability of overexpressed FT-Nrf2. In agreement with this conclusion, when FT-Nrf2 was co-expressed with unlabelled Keap1, we observed a time-dependent reduction in fluorescence lifetime of FT-Nrf2 upon sulforaphane treatment, indicative of Nrf2 stabilisation (**Fig. 2c).** Remarkably, this was apparent in both nuclear and cytoplasmic compartments, in agreement with a previous report showing that sulforaphane inhibits the ubiquitination of Nrf2 in both the cytoplasm and the nucleus [21].

It was, however, difficult to quantify this effect due to a strong cell-to-cell variability and a lack of readout for the amount of ectopically expressed Keap1 per cell. With the stoichiometry of inhibitory Keap1-Nrf2 complex of 2:1 [22], the degree of Keap1-dependent destabilisation and turnover of Nrf2 depends on their relative abundance. Transient co-expression of sfGFP-labelled Nrf2 and mCherry-labelled Keap1 that allowed visualisation of the relative levels of these two proteins in a similar system confirmed that it was highly variable among cells (**Suppl. Fig 3**). To reduce cell-to-cell variability in the levels and relative abundance of Nrf2 and Keap1, we generated a Dox-inducible bicistronic construct that combined FLIM-timer-Nrf2, or sfGFP-Nrf2 as a control, and an unlabelled Keap1, separated by two 2A peptides shown to minimise read-through[23] (**Fig. 3a**). This construct was

integrated into a genomic FRT site within Flp-In™ T-REx™ host U2OS cells (U2OS-FRT/TO cells), giving rise to cells with Dox-inducible co-expression of FT-Nrf2 (or sfGFP-Nrf2 control) protein with Keap1 from a single promoter (**Fig. 3b**). Both sfGFP- and FLIM-timer-tagged Nrf2 were efficiently stabilised by sulforaphane treatment in this system (**Fig. 3b**). Importantly, the fluorescence lifetime of FT-labelled but not of sfGFP-labelled Nrf2 was statistically significantly reduced by sulforaphane (**Fig. 3c-d**), indicative of Nrf2 stabilisation, while vehicle (acetonitrile, ACN) had no effect on the fluorescence lifetime of FT-Nrf2. Thus, FT-Nrf2 stoichiometrically co-expressed with Keap1 can act as a sensitive reporter for the efficacy of Nrf2 inducers.

Nrf2 stability is regulated primarily by Keap1-dependent cytoplasmic degradation via an N-terminal degron in Neh2 domain of Nrf2, and by $SCF^{\beta TRCP}$ -dependent degradation in the nucleus via a phosphodegron within in Neh6 domain of Nrf2 [19]. Consequently, N- and C-terminal tags might differentially affect accessibility and efficiency of the respective degrons. To assess the effect of position on the ability FLIM-timer tag to monitor Nrf2 turnover, we constructed Nrf2 C-terminally tagged with FLIM-timer (**Suppl Fig. 4a**). Our previous study suggested that such construct is likely to be functional, since C-terminal tagging did not interfere with stabilisation of Nrf2 by the Keap1-targeting inducer CDDO [24]. In the absence of co-expressed Keap1, C-terminally tagged Nrf2-FLIM-timer still accumulated in the nucleus, but it was often more stable (i.e. it had longer fluorescence lifetime) in the cytoplasm than in the nucleus (**Fig. 4a,** compare to **Fig. 2b**). The fluorescence lifetime of this construct showed an excellent negative linear correlation with mCherry/GFP ratio (**Suppl. Fig. 4b**), confirming that FLIM measurements reflected the maturation state of the fluorescence timer. Furthermore, the depletion of either a bipartite N-terminal degron for Keap1-Cul3 mediated degradation [25, 26] or a more C-terminal motif that recruits β-TrCP for $SCF^{\beta\text{-}TrCP}$ -mediated degradation [27] decreased fluorescence lifetime of Nrf2-FT (**Fig. 4b**), consistent with stabilisation of Nrf2 in the absence of these degrons. These results confirm the ability of C-terminal FLIM-timer to report on Nrf2 stability, even without Keap1 co-expression, and show that FT-timer can be used to assess differential effects of C- and N-terminal tagging on stability of fusion proteins.

2. *Monitoring mitotic exit by visualising degradation of cyclin B1***.**

We next asked whether FLIM-timer can be employed to monitor cell cycle transitions, by visualising degradation of cyclins that drive cell cycle progression. Cyclin B1 gradually accumulates during G2 stage of cell cycle reaching its highest level in mitosis (**Fig. 5a**). Cyclin B1 continues to be transcribed throughout M-phase [28], while its degradation in early mitosis is inhibited by the so-called spindle assembly checkpoint (SAC) until all chromosomes are properly attached to the mitotic spindle. Mechanistically, an active SAC prevents the Anaphase-Promoting Complex/Cyclosome (APC/C), an E3 ubiquitin ligase, from targeting cyclin B for degradation[29]. When attachment of all chromosomes is completed, satisfaction of the SAC causes an abrupt degradation of cyclin B1 by APC/C in a complex with its co-activator CDC20 that triggers mitotic exit (**Fig. 5a**). The timing and kinetics of cyclin B1 degradation is of crucial importance for understanding the regulation of cell division, karyotype stability and the efficiency of mitosis-targeting anti-cancer drugs.

We wondered whether the FLIM-timer approach could simplify the assessment of cyclin B1 degradation. In order to avoid any potential artefacts associated with overexpression, we

used CRISPR-Cas9-mediated insertion to tag the endogenous cyclin B1 with either sfGFP- or mNeonGreen-based FLIM-timer. Several additional modifications were used in the design of these constructs. First, we decided to tag cyclin B1 with FLIM-timer on the C-terminus, as previous studies had established that a C-terminal tagging of cyclin B1 does not interfere with mitotic progression or cyclin B1 degradation[30-32]. Second, following the recommendations for the design of C-terminal tFT [14], we inverted the positions of the fluorophores (**Fig. 5b and Suppl. Fig. 5a**). Third, in order to increase brightness and reduce potential premature termination of mNeonGreen that is derived from *Branchiostoma lanceolatum* [13], we codon-optimised it for mammalian expression. Finally, we removed the first methionine from all fluorophore-coding sequences to reduce potential translation initiation from these sites.

HeLa cells with mCherry-sfGFP-tagged cyclin B1 were synchronised in mitosis using nocodazole that destabilises microtubules preventing cells that enter M-phase from forming mitotic spindles. This arrests cells with high level of cyclin B1 and an active spindle checkpoint [31, 33]. The fluorescence lifetime of mitotically arrested cells was shortened to 1918.76±17.29 ps (compared with 2176.20±24.11 ps of sfGFP alone, see **Fig. 1b**), indicating that cyclin B1-FT protein is stable in these cells (**Fig 5c**). We then treated such cells with AZ 3146, a selective inhibitor of a SAC-regulating kinase Mps1[34]. We and others have previously shown that such treatment overrides SAC and causes cyclin B1 degradation and mitotic exit in the presence of nocazadole[33]. AZ 3146 triggered a clear decline in the level of fluorescent cyclin B1 in nocodazole-arrested cells (**Fig 5d,** red), confirming that AZ 3146 induced degradation of cyclin B1. Mitotic exit was confirmed by changes in cell morphology by the end of the time course. The sfGFP fluorescence lifetime of cyclin B1-mCherry-sfGFP had started to increase within 10 min of AZ 3146 addition, and reached maximal values close to that of unquenched sfGFP, indicative of fully destabilised protein, at about 30 min of treatment (**Fig. 5e,** red), while vehicle treatment did not cause any change in the fluorescence lifetime of nocodazole-arrested cells (**Fig. 5e,** black).

Similarly, HeLa cells with mCherry-mNeonGreen-tagged cyclin B1 (**Suppl. Fig 5a**) displayed strong mNeonGreen fluorescence in mitotic cells with a shortened fluorescence lifetime typical for a stable protein (**Suppl. Fig 5b,** left), compared to that of mNeonGreen alone (see **Fig. 1b**). In mitotically arrested cells, average fluorescence lifetime was 2311.32±20.33 ps, much lower than 2810.32±45.82 ps in mNeonGreen expressing cells shown in **Fig 1b**. The fluorescence intensity of mNeonGreen in nocodazole-arrested cells quickly declined upon AZ 3146 addition, reaching plateau after 40 min (**Suppl. Fig. 5c**), confirming that AZ 3146 induced degradation of cyclin B1. Unfortunately, we also observed a significant (albeit smaller) loss of mNeonGreen fluorescence intensity in mitotic cells treated with vehicle (**Suppl. Fig. 5c**, black), or in repeatedly imaged untreated mitotic cells (not shown), indicative of strong bleaching of mNeonGreen under laser illumination. AZ 3146 treatment caused a time-dependent increase in mNeonGreen fluorescence lifetime of mCherry-mNeonGreen-tagged Cyclin B1 (**Suppl. Fig. 5d**), consistent with cyclin B1 destabilisation, however the level of fluorescence in these cells quickly became too low for reliable FLIM measurements. In addition, vehicle-treated cells showed a small but measurable increase in fluorescence lifetime (**Suppl. Fig. 5d** black and data not shown) upon repeated imaging that might be caused by photobleaching.

The negligeable fluorescence intensities of interphase cells with mCherry-mNeonGreen-tagged cyclin B1 (**Suppl. Fig. 5b**, right) prevented us from comparing fluorescence lifetimes between cell cycle stages. By contrast, the intensity of endogenous cyclin B1-mCherry-sfGFP in interphase cells was sufficient to observe changes in cyclin B1 turnover throughout the cell cycle. Repeated FLIM measurements of untreated unsynchronous population of HeLa cells expressing this construct (**Fig. 5e**) allowed not only to detect the stabilised cyclin B1 in mitotic cells (asterisks), but also to observe destabilisation of cyclin B1 upon mitotic exit and cell division (red arrows) and a gradual decrease in the turnover of cyclin B1 in some of interphase cells that are presumably at G2 stage of cell cycle, apparent as a decrease in fluorescence lifetime (yellow arrow). This was not observed in cells expressing donor-only tagged CyclinB1 (**Fig. 5g** and **Suppl. Fig. 5e**).

Thus, the high brightness and photostability of sfGFP-based FLIM-timer allows its use for endogenously labelled proteins and make it suitable to monitor cyclin B1 degradation during mitotic exit.

Discussion

We present here a novel concept to use FRET as readout of fluorescence timer. Fluorescence timer applications utilise kinetics of their maturation apparent from changes in either their spectra (for single-molecule fluorescence timers) or intensity (for tandem fluorescence timers that are composed of two fluorophores with different maturation rates). We show that the FRET-accepting properties of mCherry also change with time of its maturation, allowing the use of FLIM-FRET as readout of fluorescence timer. The fluorophore maturation starts from autocatalytic cyclization of chromophore-forming tripeptide within β-barrel, followed in most GFP-like fluorophores by the rate-limiting dehydration and oxidation steps [10, 35]. In red-shifted fluorophores, additional steps are required for full maturation, though the exact mechanism differs between fluorophores [36]. A branching point at dehydration step was suggested to direct the fluorophore maturation toward formation of red fluorophores, via a blue intermediate [37]. An alternative mechanism of red fluorophore maturation proceeds via a green fluorescent state [36], and the existence of such green intermediates have been shown for DsRed and its derivative mCherry [38, 39]. Whether these intermediate states have different FRET-accepting properties has not been explored. FRET acceptor causes a non-radiative efflux of energy from a proximal donor fluorophore, on condition that the absorbance spectrum of the FRET acceptor overlaps with the emission spectrum of the FRET donor, and their respective emission and absorbance dipoles are not perpendicular to each other [6]. While it is clear that the absorbance spectra of blue intermediates should not overlap with the emission of a green FRET donor such as sfGFP, the potential of green or colourless intermediates to serve as FRET acceptors is not known. The lack of fluorescence does not necessarily preclude FRET accepting, as apparent from the existence of dark FRET acceptors [40, 41], and FRET between fluorophores of identical spectra (e.g. homo-FRET) is also possible [42]. However, the tight correlation between relative intensity of mCherry within tandem Fluorescence Timer and its ability to mediate FLIM-FRET that we observed here (**Fig. 1c** and **Fig. 4c**) suggests that none of the maturation intermediates of mCherry are able to accept FRET from the green FRET donor, and that this ability is the property of the fully mature mCherry. Whether the same is true for other red-shifted fluorophores remains to be seen.

In order to use FRET-accepting properties of mCherry as a readout of protein turnover, we combined it with a fast-maturing FRET donor within a previously described tandem fluorescence timer [4], with additional restrains designed to promote FRET (we named this construct FLIM-timer to distinguish it from other tFTs). Specifically, we ensured that the linker between the fluorophores was suitable to arrange them in a FRET-conducive way (that is, a relatively rigid linker that positions the adjacent fluorophores in a way that their dipoles are not perpendicular to each other, as this geometry promotes FRET [6]), that they are in close proximity, and that the fluorescence emission spectrum of the fast-maturing fluorophore overlaps with the fluorescence excitation spectrum of the slow-maturing fluorophore. While we have previously shown an efficient FRET between sfGFP and mCherry [7], this is, to our knowledge, the first validation of the mNeonGreen - mCherry FRET pair (see **Fig 1b**). However, despite being excellent FRET donor and having a suitably fast fluorescence maturation, the usefulness of mNeonGreen in FLIM-timer was limited by its low photostability under laser illumination (which was previously estimated at ~40% of that of mEGFP [13]). Even though we used fluorescence lifetime to measure FRET, believed to be insensitive to a low level photobleaching [5], in our experiments the photobleaching of mNeonGreen was associated with changes in fluorescence lifetime values, consistent with previously described effect of a strong photobleaching on FLIM-FRET measurements [43].
It is worth noting that systems with higher expression levels of the tagged protein and/or single imaging experiments might still benefit from mNeonGreen-based FLIM-timer as they would require lower laser power for measurements and have lower photobleaching.

Throughout this work, the fluorescence lifetime data were analysed using a single-exponential decay model. This model is a simplification, since the fluorescence lifetime of FLIM-timer in each pixel or cellular area is likely to be a combination of fluorescence lifetimes of unquenched FRET donor and FRET donor quenched to a different degree at multiple stages of acceptor maturation, - thus, it would be best described by a multiexponential or stretch-exponential decay model [44]. The presence of more than two components is indeed apparent from the partial mismatch of the 2-component model and the photon trace shown in the **Suppl. Fig 1c**. However, the simplified analysis with one-component exponential model was only marginally less fitting (compare R^2 for both models in **Suppl Fig 1c**), showed an excellent correlation with the previously used protein stability measurements (**Fig 1c**), and requires much fewer photon data than the more complex analytical models, allowing to perform FLIM acquisition at lower laser illumination intensity or for a shorter time, reducing photobleaching and loss of resolution due to cell movement. We have previously shown the validity of such simplification, confirming that analysing the 2-component FLIM with single-exponential fitting produces very similar pattern of fluorescence lifetimes [7].

The principal advantage of the method described here is that it utilises fluorescence lifetime for measuring protein turnover with fluorescence timers, which in turn makes it independent on fluorescence intensity and allows comparison between bright and dim cellular compartments. It is particularly useful for strongly compartmentalised target proteins such as Nrf2 described above. The mechanism of Nrf2 stabilisation by Nrf2 inducers is not completely understood, and one of the existing models suggests that inducer-modified Keap1 traps Nrf2 in the cytoplasm within dysfunctional Cullin3-Keap1 E3 ligase

complex, before newly synthesised Nrf2 moves to the nucleus [45]. The newly developed FLIM-timer technology made it possible for the first time to experimentally test this hypothesis. In support of the above model, our data revealed that the Nrf2 inducer sulforaphane causes Keap1-dependent cytoplasmic stabilisation of Nrf2 (**Fig. 2c**). Our approach also confirmed the contribution of Keap1-independent degradation pathways to Nrf2 turnover (**Fig. 4b**).

In conclusion, the FLIM-timer method described here greatly increases the applicability of fluorescence timers for visualisation and quantification of protein turnover, expanding it to cells with low and variable levels of the target protein. On the other hand, the current limitations of the Single Photon Counting FLIM measurement technique impose the lower limit on fluorescence intensity. FLIM technology is a fast-developing field, and recent and future advances that increase its efficiency will undoubtedly lift these limitations and expand the use of FLIM-timer to many more experimental systems.

Material and methods

Reagents

Doxycycline hyclate (Dox, Sigma/Merk, D9891), *R,S*-sulforaphane (LKT Labs, S8044), nocodazole (EMD Millipore, 487928), AZ3146 (Selleckchem, S2731). Antibodies for immunoblotting: rat monoclonal anti-Keap1, clone 144 (Millipore, MABS514, 1:10000 dilution); rabbit anti-Nrf2 rb (Cell Signalling, D1Z9C, cat Nr 12721P, 1:1000 dilution); rabbit polyclonal anti-EGFP (AbCam, ab6556, 1:1000 dilution) that detects sfGFP; anti-mCherry (Living Colors, 1:1000 dilution), mouse monoclonal anti-β-actin, clone AC-15 (Sigma, A 5441, 1:20000 dilution); anti-rabbit, anti-rat and anti-mouse IRDye800 or IRDye-680 labelled secondary antibodies (Li-COR Biosciences, 1:15000 dilution).

Plasmids

Plasmids encoding an unlabelled mouse Keap1 and fluorescently labelled mouse sfGFP-Nrf2 and mouse Keap1-mCherry (Keap1-12fl-mCherry) were described previously [7, 46]. pmCherry-N1 and pEGFP-C1 are from Clontech, sfGFP-C1 (N54579) is from Addgene, and pcDNA5-FRT/TO and pOG44 are from ThermoFisher. The construct for transient overexpression of FT-Nrf2 (sfGFP-mCherry-Nrf2) was cloned by inserting a fragment comprising a linker followed by a mCherry coding sequence excised with BsrGI from a previously described pEGFP-mCherry plasmid [20] into the BsrGI site of sfGFP-Nrf2. The plasmid for transient Nrf2-FT expression (Nrf2-sfGFP-mCherry, DU58475) was constructed by replacing the first half of mCherry sequence between AgeI and BbvCI restriction sites in a previously described Nrf2-mCherry [24] (DU58450) by the AgeI-BbvCI fragment from the above FT-Nrf2 plasmid that encompassed sfGFP, linker and the first half of mCherry. The mutant Nrf2-FT lacking C-terminal bi-partite degron for Keap1-mediated degradation (ΔNdNrf2-FT, DU58523) was generated from Nrf2-FT by sequential QuickChange mutagenesis that replaced nucleotides 76[caagacatagatcttgg]92 of Nrf2 ORF by 76[TCagacatagCtGGtgA]92 and removed nucleotides 235[gaaacaggagaa]246, thereby producing the Nrf2 protein carrying S26Q, D29A, L30G and G31E substitutions and 79[ETGE]82 depletion. The mutant Nrf2-FT lacking a more C-terminal GSK3β-dependent degron (ΔCdNrf2-FT, DU58532) was generated by deleting nucleotides 1000[gactctggcatttca]1014 of Nrf2 ORF, resulting in removal of the amino acids 334[DSGIS]338. sfGFP-Nrf2-mCherry (DU58516) was constructed by subcloning the HindIII/MfeI insert from mNrf2-mCherry containing the C-terminal portion of mNrf2 and

the mCherry open reading frame into the same sites of sfGFP-Nrf2. pcDNA5D FRT/TO sfGFP (DU58501) and pcDNA5D FRT/TO sfGFP-mCherry (DU58502) were made by PCR amplifying the sfGFP or sfGFP-linker-mCherry sequences from above Nrf2-sfGFP-mCherry (DU58475) and cloning it as a BamHI/NotI insert into the same sites of pcDNA5D FRT/TO (pcDNA5 FRT/TO (ThermoFisher) with modified multiple cloning sites, MRC-PPU reagents and services, DU41459). pcDNA5D-FRT/TO-sfGFP-AID (DU58517) and pcDNA5D-FRT/TO-sfGFP-mCherry-AID (DU58520) were made by PCR amplifying a linker-flanked AID sequence from pAID1.1-N (kind gift from Kevin Hiom) and cloning it as a NotI-NotI insert into the NotI site of above pcDNA5D FRT/TO sfGFP (DU58501) or pcDNA5D FRT/TO sfGFP-mCherry (DU58502).

To generate pcDNA5D-FRT/TO-mNeonGreen-mCherry-AID and pcDNA5D-FRT/TO-mNeonGreen-AID plasmids, mNeonGreen was PCR-amplified from synthesized mNeonGreen (BaseClear) with the primers introducing BamHI and BsrGI sites. These sites were used to replace sfGFP in above pcDNA5D-FRT/TO-sfGFP-mCherry-AID and pcDNA5D-FRT/TO-sfGFP-AID plasmids.

Plasmid for bicistronic co-expression of sfGFP-mCherry-Nrf2 with unlabelled Keap1 (pcDNA5-FRT/TO-sfGFP-mCherry-Nrf2--Keap1) was produced from pcDNA5D-FRT/TO-sfGFP-mCherry-AID by replacing “mCherry-AID” fragment by an insert comprised of mCherry-Nrf2, followed by P2A and T2A peptide sequences from pGEMT-PTE2A (kind gift of Li Qian) and followed by Keap1, in a sequential multi-step cloning. For the pcDNA5-FRT/TO-sfGFP-Nrf2--Keap1 plasmid served as a control, mCherry sequence was not included into an insert.
The constructs for endogenous tagging of Cyclin B1 with sfGFP- or mNeonGreen-based FLIM-timer were produced by Gibson assembly of the AAV_cyclin B-EYFP vector[30] with the GeneArt custom DNA fragment (ThermoFisher Scientific) containing the mCherry ORF, SGLRSRA linker, followed by either sfGFP or codon-optimised mNeonGreen ORF (all fluorophore sequences without first methionine-coding triplet), flanked by the 57-60 nucleotide overhang sequences that matched cyclin B-LHA and cyclin B-RHA from the AAV_cyclin B-EYFP modified to include BspEI, SalI and NotI restriction sites. Cyclin B1-sfGFP plasmid was made by excising mCherry from cyclin B1-mCherry-sfGFP using BspEI sites around mCherry ORF. All constructs were sequence-validated.

Cell lines
HEK293 and HeLa cells were cultured in DMEM media containing 10% heat-inactivated Fetal Bovine Serum. Early passage IMR90 cells were grown under DMEM media containing 20% heat-inactivated Fetal Bovine Serum and freshly added L-Glutamine. Flp-In™ T-REx™ host cells U2OS-FRT-TO (kind gift of Dr Laureano de la Vega) and HeLa-FRT-TO (kind gift of Prof Stephen Taylor) were maintained in DMEM media containing 10% heat-inactivated Fetal Bovine Serum. For integration of Dox-inducible clones into Flp-In™ T-REx™ host cells, cells were co-transfected with 1:1 mixture of the construct of interest cloned into pcDNA5-FRT-TO vector and pOG44 plasmid encoding Flip recombinase, using Lipofectamine 2000 (Invitrogen). The cells with successful integration were selected under 250 µg/ml hygromycin B (ThermoFisher Scientific).
Endogenous cyclin B1 was tagged using CRISPR-Cas9 knock-in strategy. HeLa-FRT-TO cells were transfected with homology arms (CyclinB-mCherry-sfGFP, CyclinB-mCherry-mNeonGreen, CyclinB-sfGFP or CyclinB-mNeonGreen), gRNA (TGTAACTTGTAAACTTGAGT)

and pcDNA5-Cas9-WT-NLS, using FuGENE HD (Promega) according to manufacturer's protocol. 5h after transfection, cells were treated with 1 μg/mL doxycycline (Sigma) for 3 days to trigger Cas9 expression. Tagged cyclin B1 cells were then enriched by FACS sorting. Sorted cells were collected and cultured for 1 week in collection media – DMEM (Gibco) supplemented with 20% FBS (Gibco), 50 μg/mL penicillin/streptomycin (Thermo Fisher), 100 μg/mL Normocin™ (InvivoGen) and 30% conditioned media (filtered from cells after 2-3 days culture).

Cell transfections and treatments

Transient transfections of cell lines were performed using calcium phosphate method as described [47] or (for IMR90) using Continuum transfection reagent (GeminiBio) following manufacturer's instructions. Prior imaging, cell culture media was replaced by phenol-free DMEM with all required supplements specific to cell line. To induce expression of integrated constructs in generated cells with Dox-inducible integrated constructs, 0.5-1 μg/ml Doxycycline hyclate (Dox, Sigma/Merk) was added to the media for more than 20 hours. Treatments added during imaging were pre-diluted in 20-100 μl of imaging media at the concentration required to achieve indicated final concentration in the sample. The same dilution of vehicle was used as a control.

Immunoblotting

Cells grown on 6-well plates were washed twice with PBS and lysed in SDS lysis buffer containing 2% SDS, 62.5 mM TrisHCl pH 6.8, 10% glycerol and protease inhibitors (cOmplete Mini, EDTA-free protease inhibitor cocktail, Roche), boiled for 2 min, sonicated and supplemented with DTT up to 100 μM final concentration and small amount of Bromophenol Blue. 10 μg of lysates were separated on 4-12% pre-cast BisTris NuPAGE gels (Invitrogen) under MOPS running buffer alongside a PageRuler™ protein ladder (ThermoFisher Scientific, 26616) and transferred onto Amersham™ Protran® Premium 0.45 μm Nitrocellulose membrane under transfer buffer containing 25 mM Tris, 129 mM Glycine and 20% Methanol. Membranes were stained with 1% Ponceau S in 5% acetic acid to confirm equal transfer, de-stained and blocked in 5% non-fat milk in PBST (PBS supplemented with 0.1% Tween 20) for 1 h before blotting with primary antibodies diluted to indicated concentration in above blocking solution overnight at 4^0C. Membranes were washed in PBST, incubated with appropriate secondary antibodies diluted 1:15000 in blocking solution for 1 h at room temperature, washed again and scanned using Odyssey CLx Infrared Imaging System. Alternatively, blots were incubated with 1:5000 diluted HRP-labelled secondary antibody followed by development with ECL reagents (Amersham) and exposure to film.

Imaging

Life cells were imaged on LSM 710 (Zeiss) confocal microscope operated by ZEN software (Zeiss) equipped with dark environmental chamber maintained at 37^0C and a humidified source of 5% CO_2. Cell growing on glass-bottom dishes (35 mm FluoroDishes, World Precision Instruments, or 35 mm 4-compartment CELLview dishes, Greiner Bio-One) were held in heated Petri-dish holder insert and imaged with 488 nm (for EGFP, sfGFP or mNeonGreen) or 594 nm (for mCherry) confocal lasers using 63x/1.4NA oil immersion objective. Within each experiment, the laser settings and acquisition parameters were

identical between samples. Images were processed to adjust displayed intensities, generate maximal intensity projections, add annotations and create movies in ImageJ/FIJI or OMERO.

FLIM acquisition and analysis

Fluorescence lifetime was measured using SPC-150 Time-Correlated Single Photon Counter (TCSPC) module (Becker&Hickl) attached to LSM 710 microscope (Zeiss) equipped with either InTune pulsed laser with repetition rate 40 MHz and tunable wavelength (Zeiss) or 2-photon Chameleon laser with pulse repetition rate 80 MHz (Coherent) and HPM-100-40GaAsP detector that feeds to TCSPC module. FLIM data acquisition is operated by SPCM software (Becker&Hickl) controlling TCSPC module. sfGFP fluorescence lifetime was measured at 490 nm (InTune laser) or 920 nm (2-photon laser) wavelength and the filters suitable for GFP. Fluorescence lifetime of mNeonGreen was measured with InTune laser at 490 nm. Each measurement was acquired for 40-120 sec with laser intensities adjusted to achieve Constant Fraction Discriminator (CFD) rate between $5x10^5$ and $1x10^6$ events per second, with time resolution of 256 time-channels and spatial resolution of 512x512 or 256x256 pixels. The duration of acquisition and resolution were kept constant among all samples of the same experiment. FLIM generated the cumulative photon traces within each pixel of the image, which can be used to determine fluorescence lifetime(s) by fitting an appropriate exponential decay model (generic formula 1 or 2 below).

One-exponential decay model: $F(t) = ae^{-t/\mathrm{t}}$ (1)

Two-exponential decay model: $F(t) = a1e^{-\frac{t}{\mathrm{t1}}} + a2e^{-t/\mathrm{t2}}$ (2)

where τ, $\tau 1$ and $\tau 2$ are fluorescence lifetime components, $a1$ and $a2$ are the relative amplitudes of each component with $a1 + a2 = 100\%$, and t is an independent variable.

This analysis was performed within SPCImage (Becker&Hickl), where fluorescence lifetime was determined by fitting 1- or 2-component exponential decay models adjusted to remove the signal from Instrument Response Function (IRF) by deconvolution to the binned data. For the pixel-by-pixel analysis (used for generating images or calculating mean fluorescence lifetimes and changes in fluorescence lifetime as indicated), bin 3 or 4 was used. Alternatively, global binning was used as previously described [7] by pulling together the data from all pixels within an outlined region of interest (nucleus, cytoplasm or entire cell). For 2-component analysis, the second component was fixed at the average value obtained by measuring the FRET donor-only controls, and the amplitude weighted average fluorescence lifetime was calculated within the SPCImage software following formula 3:

$$\mathrm{tm} = \frac{a1*\mathrm{t1} + a2*\mathrm{t2}}{a1+a2} \quad (3)$$

FRET efficiency (E) was calculated from 2-component exponential decay fitting as

$$E = 1 - \frac{tm}{\mathrm{t2}} \quad (4)$$

where tm is amplitude weighted average fluorescence lifetime and $\tau 2$ is the longer fluorescence lifetime component corresponding to fluorescence lifetime of FRET-donor only control.

Alternatively, the binned photon traces were exported from SPCImage and further analysed in R, where the 1- or 2-component exponential decay models were fitted to the same

dataset after removing the initial portion of the curve containing IRF, plotted together and compared using ANOVA. Goodness of fit for each model was calculated in R as (5)

$$1 - RSS/TSS \quad (5)$$

where *RSS* is a residual sum of squares, and *TSS* is total sum of squares.

The correlations between sfGFP fluorescence lifetime or FRET efficiency and the mCherry/GFP ratio were performed in R using fluorescence lifetimes values obtained with fitting the indicated model to the globally binned (pooled) FLIM data from nuclear or cytoplasmic cellular regions, and the mCherry/GFP ratio values calculated in OMERO within the same regions of the cells re-imaged by confocal microscopy in the instrument that permits sequential FLIM and confocal imaging of the same specimen.

For calculating CV in each type of measurement, sequential FLIM and confocal images of the same cells were analysed using pixel-by-pixel approach. The data files containing either fluorescence lifetimes obtained by 1-component fitting in each pixel of the image within outlined cellular area, or the number of photons (measure of GFP intensity) detected in the same pixels were exported from SPCImage and combined into matrix. Similarly, a matrix containing the mCherry/GFP intensity ratio and GFP intensity in each pixel of the same cellular area was constructed from the confocal image of the same cells. Both matrices were analysed in R, whereby pixels of similar GFP intensities were grouped into 37 bins of equal width, and the CV for fluorescence lifetime or mCherry/GFP ratio for pixels within each bin was calculated as CV = standard deviation/mean x 100. The obtained values were plotted against the middle intensity of each bin, normalised to the average GFP intensity of the entire cellular area. Time-lapse FLIM was performed as previously described [47]. To calculate intensity-independent changes in fluorescence lifetime or analyse FLIM time-lapses, the data from SPCImage were exported, processed in ImageJ and analysed within FLIMDAST (https://github.com/DinaDikovskaya/FLIMDAST) following a previously described pipeline [47]. Within each experiment, all FLIM data/images were acquired using the same optical settings and processed identically (including magnification factor). The intensity images represent the map of photon numbers acquired in each pixel.

Data analysis

Data were assembled in Excel and analysed and plotted in R. Goodness of fit (R^2), Pearson correlation coefficient (r) and p-values were calculated in R. P-values were determined using Welch two sample t-test.

Acknowledgements

We thank Dr Li Qian, Department of Pathology and Laboratory Medicine, The University of North Carolina, Chapel Hill, USA for pGEMT-PTE2A plasmid and Prof Kevin Hiom, University of Dundee, UK, for pAID1.1-N plasmid. We thank Dr Laureano de la Vega, University of Dundee, UK, for U2OS-FRT-TO cells, and Prof Stephen Taylor, Cancer Research Centre, Manchester, UK, for HeLa-FRT-TO cells. We would like to acknowledge the Flow Cytometry and Cell Sorting Facility at the University of Dundee for cell sorting, which is supported by the Wellcome Trust grant (097418/Z/11/Z). We thank Prof Miratul M. K. Miqit for his contribution in obtaining funding and for helpful discussion, and Marek Gierlinski (School of Life Sciences, University of Dundee) for advice on data analysis. This project was funded by Tenovus Scotland large grant (T17/14), Biotechnology and Biological Sciences Research

Council grant (BB/T017546/1), Medical Research Council Doctoral Training Programme (MR/K501384), and Wellcome Trust ISSF bridging grant (204816/Z/16/Z). Kanade Shiga was funded by Japan Student Services Organization (JASSO), grant number HTA1910900401.

Author Contributions

DD and ATD conceived and designed the study, ATS made a substantial contribution to the experimental design. DD, CB, KS, AC, MH and RT generated and validated plasmids and cell lines used in this study. DD and CB performed the experiments. DD analysed the data and wrote the manuscript, and ATD and ATS edited the manuscript. All authors read and approved the manuscript.

Competing Interests

The authors declare no competing interests

References

1. Terskikh, A. et al. "Fluorescent timer": protein that changes color with time. *Science* **290**, 1585-1588 (2000).
2. Subach, F.V. et al. Monomeric fluorescent timers that change color from blue to red report on cellular trafficking. *Nat Chem Biol* **5**, 118-126 (2009).
3. Tsuboi, T., Kitaguchi, T., Karasawa, S., Fukuda, M. & Miyawaki, A. Age-dependent preferential dense-core vesicle exocytosis in neuroendocrine cells revealed by newly developed monomeric fluorescent timer protein. *Mol Biol Cell* **21**, 87-94 (2010).
4. Khmelinskii, A. et al. Tandem fluorescent protein timers for in vivo analysis of protein dynamics. *Nat Biotechnol* **30**, 708-714 (2012).
5. Berezin, M.Y. & Achilefu, S. Fluorescence lifetime measurements and biological imaging. *Chem Rev* **110**, 2641-2684 (2010).
6. Vogel, S.S., Thaler, C. & Koushik, S.V. Fanciful FRET. *Sci STKE* **2006**, re2 (2006).
7. Dikovskaya, D., Appleton, P.L., Bento-Pereira, C. & Dinkova-Kostova, A.T. Measuring the Interaction of Transcription Factor Nrf2 with Its Negative Regulator Keap1 in Single Live Cells by an Improved FRET/FLIM Analysis. *Chem Res Toxicol* **32**, 500-512 (2019).
8. Day, R.N. & Davidson, M.W. Fluorescent proteins for FRET microscopy: monitoring protein interactions in living cells. *Bioessays* **34**, 341-350 (2012).
9. Bajar, B.T., Wang, E.S., Zhang, S., Lin, M.Z. & Chu, J. A Guide to Fluorescent Protein FRET Pairs. *Sensors (Basel)* **16** (2016).
10. Grigorenko, B.L., Krylov, A.I. & Nemukhin, A.V. Molecular Modeling Clarifies the Mechanism of Chromophore Maturation in the Green Fluorescent Protein. *J Am Chem Soc* **139**, 10239-10249 (2017).
11. Balleza, E., Kim, J.M. & Cluzel, P. Systematic characterization of maturation time of fluorescent proteins in living cells. *Nat Methods* **15**, 47-51 (2018).
12. Pedelacq, J.D., Cabantous, S., Tran, T., Terwilliger, T.C. & Waldo, G.S. Engineering and characterization of a superfolder green fluorescent protein. *Nat Biotechnol* **24**, 79-88 (2006).
13. Shaner, N.C. et al. A bright monomeric green fluorescent protein derived from Branchiostoma lanceolatum. *Nat Methods* **10**, 407-409 (2013).

14. Khmelinskii, A. et al. Incomplete proteasomal degradation of green fluorescent proteins in the context of tandem fluorescent protein timers. *Mol Biol Cell* **27**, 360-370 (2016).
15. Kobayashi, A. et al. Oxidative stress sensor Keap1 functions as an adaptor for Cul3-based E3 ligase to regulate proteasomal degradation of Nrf2. *Mol Cell Biol* **24**, 7130-7139 (2004).
16. He, X., Chen, M.G., Lin, G.X. & Ma, Q. Arsenic induces NAD(P)H-quinone oxidoreductase I by disrupting the Nrf2 x Keap1 x Cul3 complex and recruiting Nrf2 x Maf to the antioxidant response element enhancer. *J Biol Chem* **281**, 23620-23631 (2006).
17. Yamamoto, M., Kensler, T.W. & Motohashi, H. The KEAP1-NRF2 System: a Thiol-Based Sensor-Effector Apparatus for Maintaining Redox Homeostasis. *Physiol Rev* **98**, 1169-1203 (2018).
18. Cuadrado, A. et al. Therapeutic targeting of the NRF2 and KEAP1 partnership in chronic diseases. *Nat Rev Drug Discov* **18**, 295-317 (2019).
19. Robledinos-Anton, N., Fernandez-Gines, R., Manda, G. & Cuadrado, A. Activators and Inhibitors of NRF2: A Review of Their Potential for Clinical Development. *Oxid Med Cell Longev* **2019**, 9372182 (2019).
20. Baird, L., Lleres, D., Swift, S. & Dinkova-Kostova, A.T. Regulatory flexibility in the Nrf2-mediated stress response is conferred by conformational cycling of the Keap1-Nrf2 protein complex. *Proc Natl Acad Sci U S A* **110**, 15259-15264 (2013).
21. Li, Y., Paonessa, J.D. & Zhang, Y. Mechanism of chemical activation of Nrf2. *PLoS One* **7**, e35122 (2012).
22. Iso, T., Suzuki, T., Baird, L. & Yamamoto, M. Absolute Amounts and Status of the Nrf2-Keap1-Cul3 Complex within Cells. *Mol Cell Biol* **36**, 3100-3112 (2016).
23. Liu, Z. et al. Systematic comparison of 2A peptides for cloning multi-genes in a polycistronic vector. *Sci Rep* **7**, 2193 (2017).
24. Baird, L. & Dinkova-Kostova, A.T. Diffusion dynamics of the Keap1-Cullin3 interaction in single live cells. *Biochem Biophys Res Commun* **433**, 58-65 (2013).
25. Katoh, Y. et al. Evolutionary conserved N-terminal domain of Nrf2 is essential for the Keap1-mediated degradation of the protein by proteasome. *Arch Biochem Biophys* **433**, 342-350 (2005).
26. McMahon, M., Thomas, N., Itoh, K., Yamamoto, M. & Hayes, J.D. Dimerization of substrate adaptors can facilitate cullin-mediated ubiquitylation of proteins by a "tethering" mechanism: a two-site interaction model for the Nrf2-Keap1 complex. *J Biol Chem* **281**, 24756-24768 (2006).
27. Chowdhry, S. et al. Nrf2 is controlled by two distinct beta-TrCP recognition motifs in its Neh6 domain, one of which can be modulated by GSK-3 activity. *Oncogene* **32**, 3765-3781 (2013).
28. Sciortino, S. et al. The cyclin B1 gene is actively transcribed during mitosis in HeLa cells. *EMBO Rep* **2**, 1018-1023 (2001).
29. Rudner, A.D. & Murray, A.W. The spindle assembly checkpoint. *Curr Opin Cell Biol* **8**, 773-780 (1996).
30. Akopyan, K. et al. Assessing kinetics from fixed cells reveals activation of the mitotic entry network at the S/G2 transition. *Mol Cell* **53**, 843-853 (2014).
31. Clute, P. & Pines, J. Temporal and spatial control of cyclin B1 destruction in metaphase. *Nat Cell Biol* **1**, 82-87 (1999).

32. Shaltiel, I.A. et al. Distinct phosphatases antagonize the p53 response in different phases of the cell cycle. *Proc Natl Acad Sci U S A* **111**, 7313-7318 (2014).
33. Saurin, A.T., van der Waal, M.S., Medema, R.H., Lens, S.M. & Kops, G.J. Aurora B potentiates Mps1 activation to ensure rapid checkpoint establishment at the onset of mitosis. *Nat Commun* **2**, 316 (2011).
34. Liu, X. & Winey, M. The MPS1 family of protein kinases. *Annu Rev Biochem* **81**, 561-585 (2012).
35. Strongin, D.E. et al. Structural rearrangements near the chromophore influence the maturation speed and brightness of DsRed variants. *Protein Eng Des Sel* **20**, 525-534 (2007).
36. Subach, F.V. & Verkhusha, V.V. Chromophore transformations in red fluorescent proteins. *Chem Rev* **112**, 4308-4327 (2012).
37. Moore, M.M., Oteng-Pabi, S.K., Pandelieva, A.T., Mayo, S.L. & Chica, R.A. Recovery of red fluorescent protein chromophore maturation deficiency through rational design. *PLoS One* **7**, e52463 (2012).
38. Gross, L.A., Baird, G.S., Hoffman, R.C., Baldridge, K.K. & Tsien, R.Y. The structure of the chromophore within DsRed, a red fluorescent protein from coral. *Proc Natl Acad Sci U S A* **97**, 11990-11995 (2000).
39. Hebisch, E., Knebel, J., Landsberg, J., Frey, E. & Leisner, M. High variation of fluorescence protein maturation times in closely related Escherichia coli strains. *PLoS One* **8**, e75991 (2013).
40. Ganesan, S., Ameer-Beg, S.M., Ng, T.T., Vojnovic, B. & Wouters, F.S. A dark yellow fluorescent protein (YFP)-based Resonance Energy-Accepting Chromoprotein (REACh) for Forster resonance energy transfer with GFP. *Proc Natl Acad Sci U S A* **103**, 4089-4094 (2006).
41. Murakoshi, H., Shibata, A.C.E., Nakahata, Y. & Nabekura, J. A dark green fluorescent protein as an acceptor for measurement of Forster resonance energy transfer. *Sci Rep* **5**, 15334 (2015).
42. Yeow, E.K. & Clayton, A.H. Enumeration of oligomerization states of membrane proteins in living cells by homo-FRET spectroscopy and microscopy: theory and application. *Biophys J* **92**, 3098-3104 (2007).
43. Tramier, M., Zahid, M., Mevel, J.C., Masse, M.J. & Coppey-Moisan, M. Sensitivity of CFP/YFP and GFP/mCherry pairs to donor photobleaching on FRET determination by fluorescence lifetime imaging microscopy in living cells. *Microsc Res Tech* **69**, 933-939 (2006).
44. Lee, K.C. et al. Application of the stretched exponential function to fluorescence lifetime imaging. *Biophys J* **81**, 1265-1274 (2001).
45. Baird, L., Swift, S., Lleres, D. & Dinkova-Kostova, A.T. Monitoring Keap1-Nrf2 interactions in single live cells. *Biotechnol Adv* **32**, 1133-1144 (2014).
46. McMahon, M., Itoh, K., Yamamoto, M. & Hayes, J.D. Keap1-dependent proteasomal degradation of transcription factor Nrf2 contributes to the negative regulation of antioxidant response element-driven gene expression. *J Biol Chem* **278**, 21592-21600 (2003).
47. Dikovskaya, D. & Dinkova-Kostova, A.T. Measuring Changes in Keap1-Nrf2 Protein Complex Conformation in Individual Cells by FLIM-FRET. *Curr Protoc Toxicol* **85**, e96 (2020).

Figures

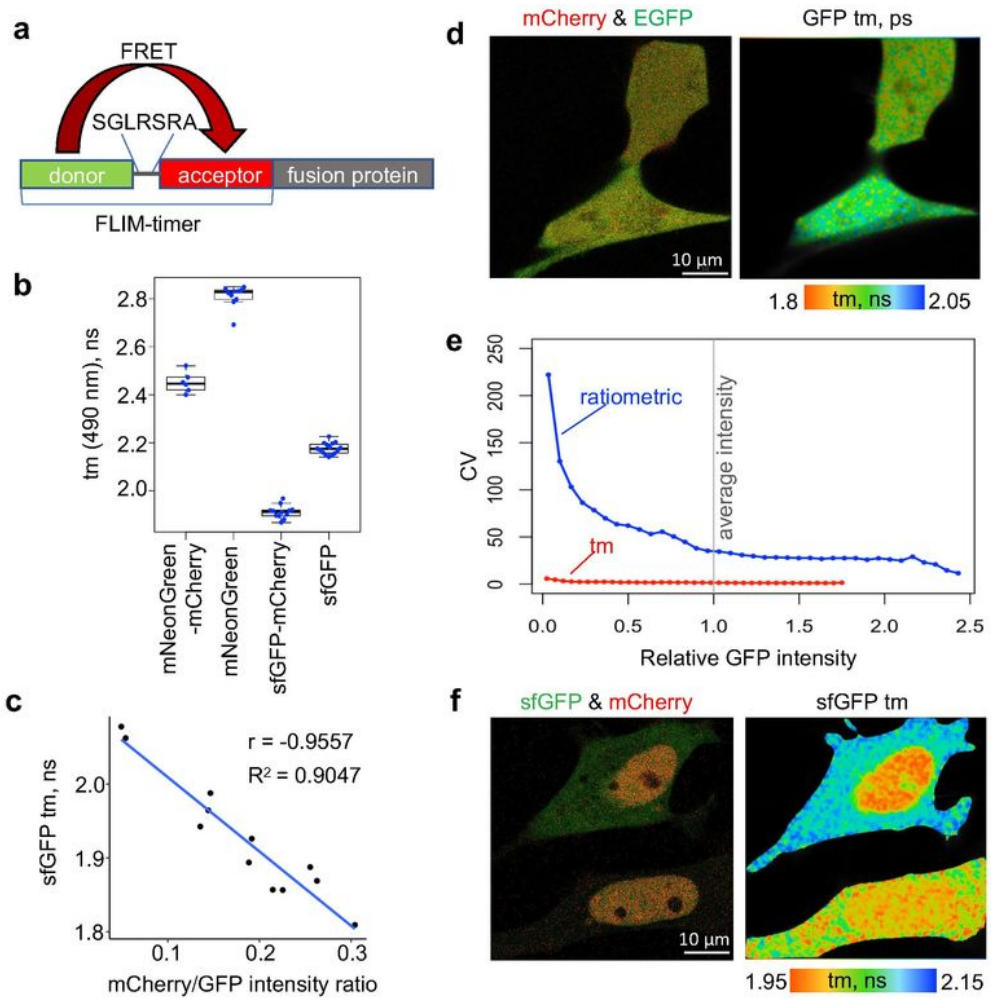

Figure 1. FLIM-based fluorescence timer for measuring protein turnover. **a,** Schematic of a protein labelled with FLIM-timer tag composed of the fast-maturing FRET donor and the slower maturing FRET acceptor, linked by a linker peptide. FRET between tag components shortens the fluorescence lifetime of the FRET donor and serves as readout for protein turnover. **b,** Fluorescence lifetimes of mNeonGreen- or sfGFP-based FLIM-timers and the appropriate mNeonGreen or sfGFP control constructs in Dox-induced HeLa-FRT/TO cells measured using InTune laser. Global fluorescence lifetime (tm) determined in entire cellular areas as described [7] are shown as dots, boxes outline the data range within lower and upper quartiles, thick line marks median and whiskers extend to the highest and lowest values excluding outliers. **c,** Strong negative correlation between ratiometric and FLIM-based measurements shown by Pearson Correlation Coefficient (r) and a slope of the linear regression fitted to the data with the high goodness of fit (R^2). Dots are globally binned sfGFP fluorescence lifetime (tm) and the mCherry/sfGFP fluorescence intensities ratios measured in the same nuclear or cytoplasmic areas of HeLa cells transiently transfected with sfGFP-mCherry-Nrf2. Fluorescence lifetime acquired with 2-photon laser, followed by confocal imaging. **d**, HEK293 cells transfected with EGFP-mCherry imaged with confocal laser in GFP and mCherry channels (left panel, mCherry in red and EGFP in green) followed by FLIM with InTune laser (right panel, GFP tm color-coded as shown underneath). **e**, The pixels within cellular areas shown in **d** were grouped by their GFP channel intensities normalised to respective average values of cellular area (vertical grey line) into 37 equal intensity bins, and the Coefficient of Variation (CV) calculated for each bin was plotted against mean bin intensity. **f,** Confocal image of HeLa cells transfected with sfGFP-mCherry-Nrf2 displayed as an overlay of sfGFP (green) and mCherry (red) channels (left panel) or as a fluorescence lifetime map obtained using FLIM (right). The false colours correspond to the tm values as shown underneath. Imaging and FLIM acquisition as in **d**. See also **Suppl Fig 1**.

Figure 1

See image above for figure legend.

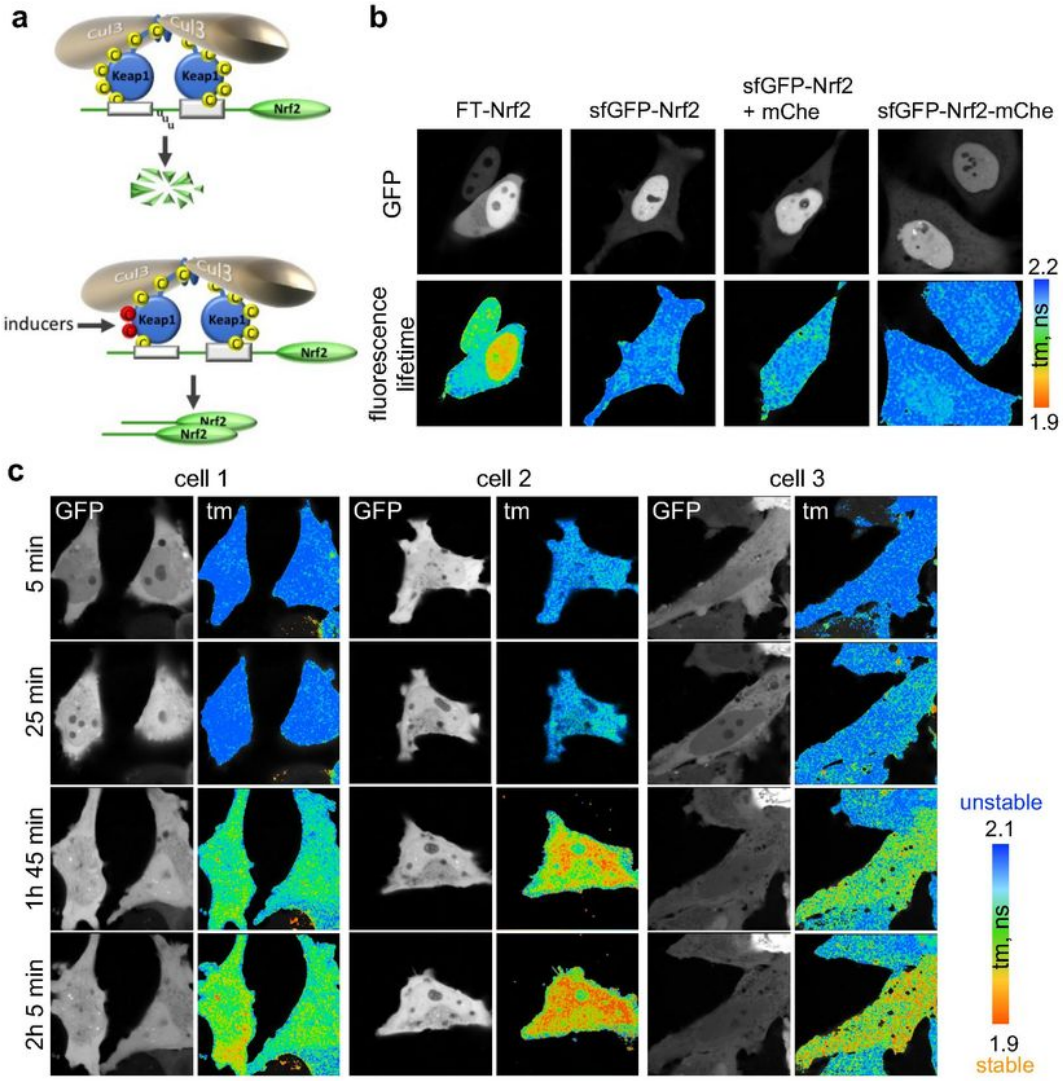

Figure 2. Measuring Nrf2 turnover using N-terminal FLIM-timer tag. **a,** Schematics of Nrf2 regulation by Keap1. At basal conditions (top), Nrf2 is targeted for proteosomal degradation by Cullin3–RING ubiquitin E3 ligase (CRL3) in a complex with its adaptor Keap1 that recruits Nrf2 to CRL3. Modifications of sensor cysteines in Keap1 by natural or pharmacological oxidants or electrophiles (inducers) inhibit CRL3 - mediated degradation of Nrf2 (bottom), which stabilises Nrf2 and initiates oxidative stress response. **b,** Photon numbers (top panels) and fluorescence lifetime heat maps (bottom panels) of HeLa cells transiently transfected with sfGFP-mCherry-Nrf2, sfGFP-Nrf2 with or without co-transfection with free mCherry, or sfGFP-Nrf2-mCherry, as indicated. The colour coding for the fluorescence lifetime images is shown on the right. FLIM acquisition here and below as in **Fig. 1f**. **c,** Photon numbers (left panels, GFP) and fluorescence lifetime heat maps (right panels, tm) in HeLa cells co-expressing sfGFP-mCherry-Nrf2 and Keap1, over the 125 min course of treatment with 5 μM sulforaphane. The colour coding for the fluorescence lifetime is shown on the right. See also **Suppl Fig. 2**.

Figure 2

See image above for figure legend.

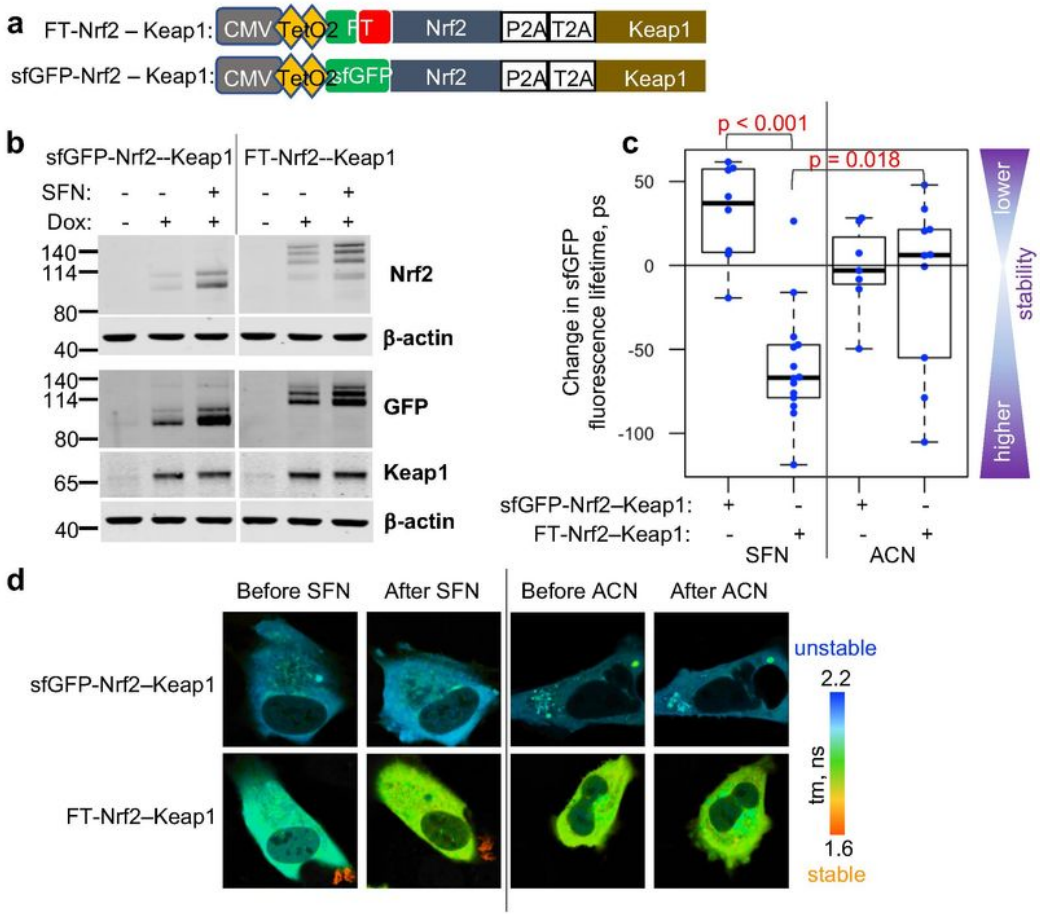

Figure 3. Measuring turnover of FLIM-Timer tagged Nrf2 stoichiometrically co-expressed with Keap1. **a,** Bicistronic constructs for Dox-inducible co-expression of sfGFP-mCherry-Nrf2 (FT-Nrf2) or sfGFP-Nrf2 with unlabelled Keap1 at a constant ratio. A sfGFP-mCherry (FLIM-timer) or sfGFP upstream of Nrf2 coding sequence is followed by two 2A peptides and a Keap1 coding sequence cloned into pcDNA5-FRT/TO vector (a part of Flp-In™ T-REx™ system) under vector's CMV promoter controlled by two Dox-sensitive TetO2 elements. **b,** U2OS-FRT/TO cells (Flp-In™ T-REx™ host U2OS cells with integrated FRT site and a Tet-repressor) with stably integrated FT-Nrf2—Keap1 or sfGFP-Nrf2—Keap1 constructs shown in **a** were either left untreated or induced with Dox for >20 h. Dox-induced cells were further treated with 5 μM sulforaphane (SFN) for 3 h or left untreated. Cells were immunoblotted for Nrf2, GFP or Keap1, with b-actin as a loading control. **c,** Fluorescence lifetime of FT-Nrf2-expressing U2OS-FRT/TO cells was significantly reduced upon SFN treatment, consistent with its stabilisation. U2OS-FRT/TO cells with stably integrated constructs shown in panel a were Dox-induced for 3 days and FLIM was measured before and after addition of either 5 μM sulforaphane (SFN) or equivalent volume of vehicle (acetonitrile, ACN) for 2 h. Each dot represents treatment-induced change in fluorescence lifetime in an individual cell, corrected for any fluorescence intensity bias as described [47]. Median shown as thick lines, and boxes outline 75 percentiles of samples as in **Fig. 1b**. **d,** Representative fluorescence lifetimes (tm) colour maps of cells quantified in **c**, before and after indicated treatment. Colour key is given on the right. See also **Suppl. Fig. 3.**

Figure 3

See image above for figure legend.

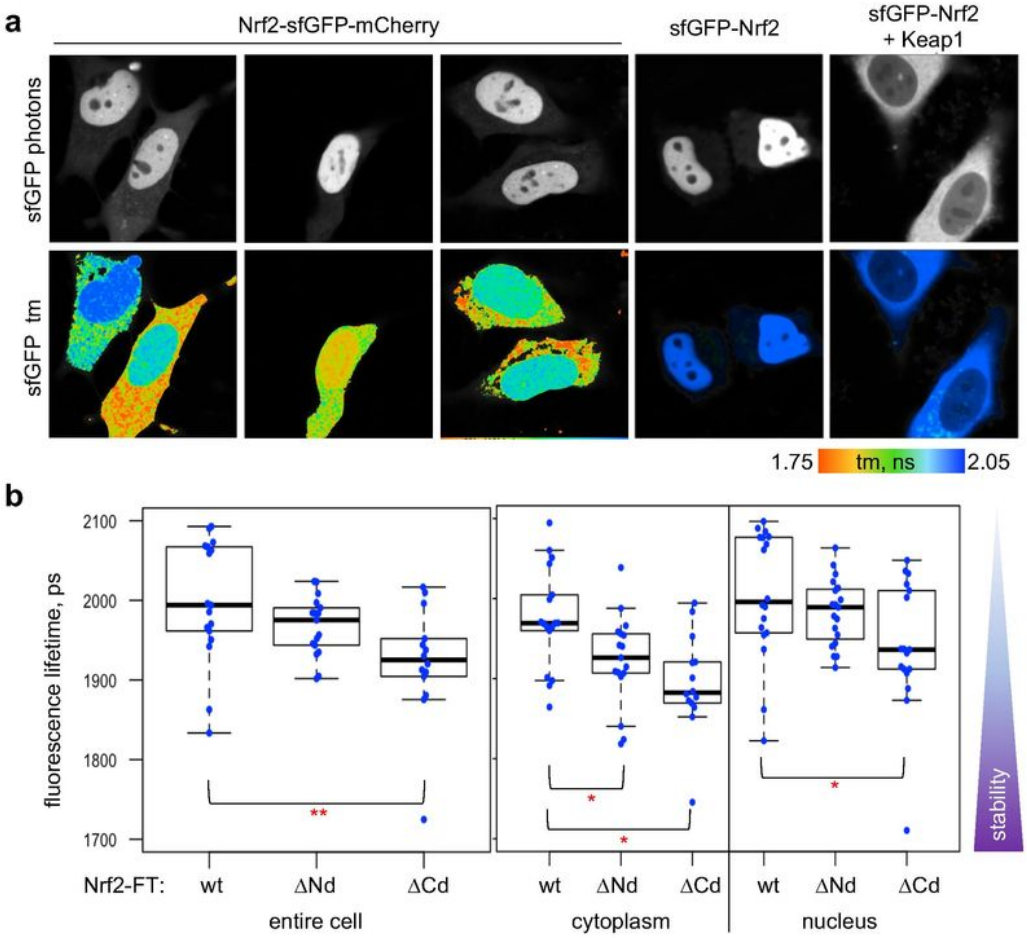

Figure 4. Measuring Nrf2 turnover with C-terminal FLIM-timer tag. **a,** Photon numbers (top) and fluorescence lifetime (tm, bottom) of HeLa cells transiently expressing Nrf2-sfGFP-mCherry (left three panels) or donor-only control sfGFP-Nrf2 (with and without Keap1, right two panels). The colour map for fluorescence lifetime is shown underneath. Note that Keap1-mediated destabilisation does not alter fluorescence lifetime of donor-only control. FLIM acquisition as in **Fig. 1c. b,** Fluorescence lifetimes of HeLa cells transfected with wild-type Nrf2 (wt) or mutant Nrf2 lacking either both DLG and ETGE motifs of N-terminal Keap1-dependend degron (DNd) or DSGIS motif serving as a C-terminal phospho-degron for b-TrCP-dependent degradation (DCd), tagged with FLIM-timer sfGFP-mCherry at its C-terminus, were measured using FLIM. Each dot represents mean fluorescence lifetime of entire cell (left) or cytoplasmic or nuclear region (right), and the boxplots show the data distribution as in **Fig. 1b.** Reduced fluorescence lifetime in Nrf2 mutants, corresponds to a more stable protein. Significant differences are indicated by asterisks: * - p<0.05, **- p<0.01. FLIM acquisition as in **Fig. 1c**. See also **Suppl Fig 4**.

Figure 4

See image above for figure legend.

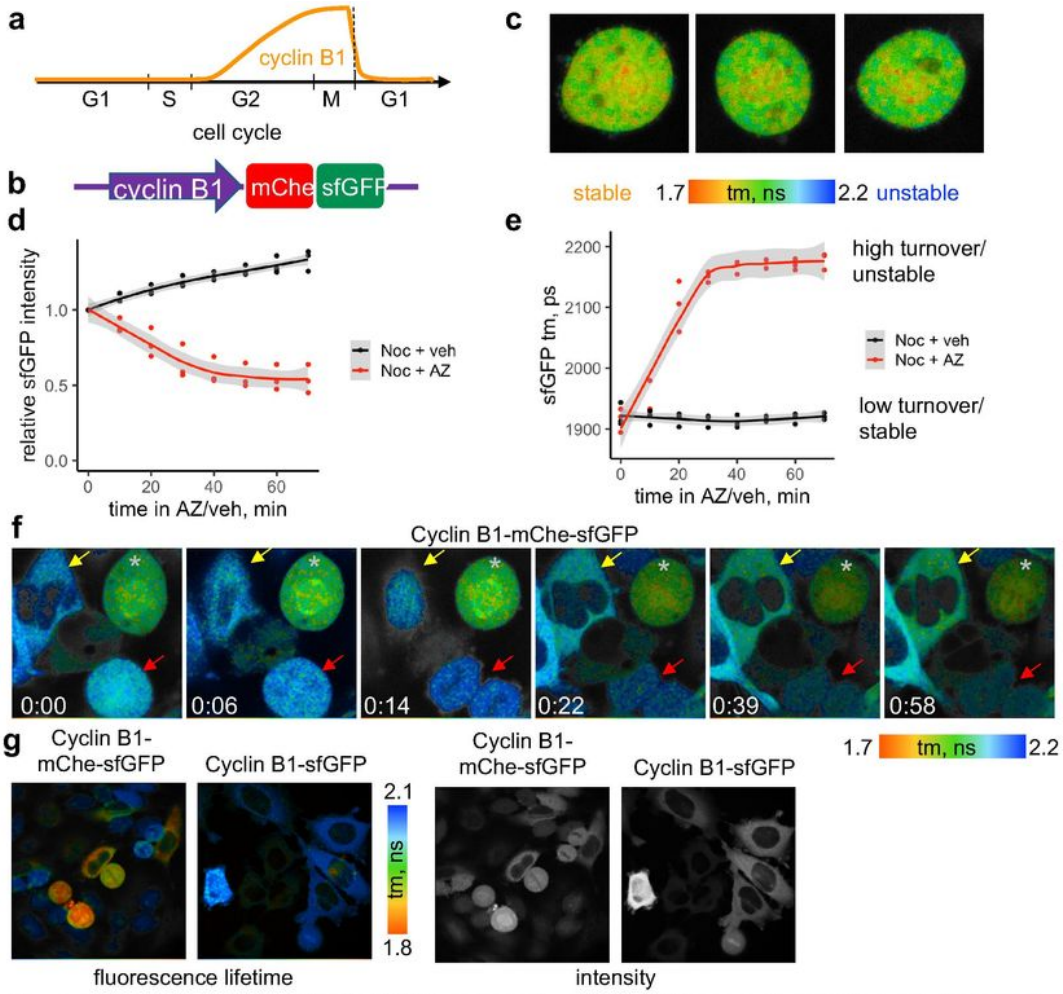

Figure 5. Monitoring mitotic exit with FLIM-timer tagged cyclin B. **a,** Changes of cyclin B1 levels during cell cycle. **b,** Cyclin B1 tagging strategy. Endogenous cyclin B1 in HeLa cells tagged using CRISPR-CAS9 with mCherry-sfGFP, separated by 7 amino-acid linker as in **Fig 1a**. **c,** Examples of fluorescence lifetime (tm) in nocodazole-arrested cells expressing cyclin B1-mCherry-sfGFP. The tm values are color-coded as shown underneath. Tm here and below was measured using InTune laser at 490 nm excitation. **d-e,** HeLa cells expressing cyclin B1-mCherry-sfGFP were treated for 1 h with Nocodazole prior addition of 1.25 μM AZ 3146 or equal volume of DMSO (veh) for 70 min. Mitotic (rounded) cells were followed by a time-lapse FLIM and normalised sfGFP fluorescence intensity (**d**) or the mean fluorescence lifetime (**e**) in each cell were plotted against time of treatment. Dots are individual cell values, the lines depict fitted local polynomial regression curve with the 95% confidence interval shown as grey shading. **f,** Time course FLIM of unsynchronised culture of HeLa cells expressing cyclin B1 endogenously tagged with mCherry-sfGFP. The intensity maps are color-coded to show fluorescence lifetimes as shown underneath. The time shown as hour:min from the start of the imaging. A cell that remains in mitosis throughout the time course is marked with asterisk; a red arrow points to a cell that exits mitosis and divides; and the yellow arrow shows to a large interphase cell that reduces fluorescence lifetime and increases its intensity over the time course, consistent with G2 stage of cell cycle. **g**, Reduced fluorescence lifetime is not observed in mitotic cells overexpressing donor-only control, Cyclin B1-sfGFP. FLIM was acquired in unsynchronised culture of HeLa cells expressing cyclin B1 endogenously tagged with either mCherry-sfGFP (left) or sfGFP(right). Tm maps are on the left two panels with color-coding shown on the right, and the sfGFP intensity (photon number maps) are on the right two panels. Note that mitotic cells (yellow arrows) display low fluorescence lifetime only in the Cyclin B1-mCherry-sfGFP expressing and not in Cyclin B1-sfGFP expressing sample. See also **Suppl Fig 5**.

Figure 5

See image above for figure legend.

Supplementary Files

This is a list of supplementary files associated with this preprint. Click to download.

- SupplFiguresDikovskayaetalCB.pdf